Available online at www.sciencedirect.com

ScienceDirect

IFAC Papers Online CONFERENCE PAPER ARCHIVE

IFAC-PapersOnLine 48-15 (2015) 389–394

On-board Thermal Fault Diagnosis of Lithium-ion Batteries For Hybrid Electric Vehicle Application

Satadru Dey*. Zoleikha Abdollahi Biron*. Sagar Tatipamula*. Nabarun Das*. Sara Mohon*. Beshah Ayalew*. Pierluigi Pisu*

**Clemson University – International Center for Automotive Research, Greenville, SC 29607 USA (e-mails: {satadrd, zabdoll, statipa, nabarud, smohon, beshah, pisup}@clemson.edu).*

Abstract: Lithium-ion batteries with different applications in industries need to be safe, reliable and long-lasting energy storage systems. The internal temperature of the battery, which is higher and more critical compared to the surface temperature, can be affected by internal thermal failures. Hence, internal temperature estimation and fault diagnosis is necessary for Lithium-ion batteries to avoid the problem of overheating. In this paper, a Luenberger observer is designed to detect and isolate three main thermal failures in the battery, consisting of thermal runaway, convective cooling resistance fault, and internal thermal resistance fault. The primary residuals generated by the observer are fed into two designed filters to create secondary residuals. By using the secondary residuals, an estimation of effect of the faults on the system can be obtained.

Keywords: Lithium-ion Batteries, Fault Diagnosis, Thermal Failure, Observer.

1. INTRODUCTION

Lithium-ion batteries are used extensively in electrified transportation such as hybrid electric vehicle (HEV) applications as well as stationary energy storage for power grids (see Divya (2009)). Despite being a promising candidate for energy storage solutions, these batteries still suffer from safety and reliability issues. One of the key critical safety aspects in Lithium-ion batteries is the thermal instability. To resolve this issue, advanced battery management systems should be designed with intelligent thermal management strategies that can prevent thermal failures. One of the possible ways to prevent such thermal failures lies in early detection and accommodation of thermal faults in the battery. In this paper, we propose a diagnostics scheme for detection and isolation of some thermal faults along with estimating some characteristics of the fault effects.

Several thermal modelling strategies for Lithium-ion batteries have been presented in literature. The first category of the thermal models possess high accuracy due to their predictive ability of the temperature distribution inside the battery (see Hallaj et al, (1999) and Maleki et al (2003) and Gu et al (2000)). However, this accuracy comes with the disadvantage of high computation burden making them less suitable for real-time applications. The second category of models which predict the lumped average temperature of the cell, are computationally efficient for real-time purposes at the cost of lower accuracy (see Smith et al (2006) and Forgez et al (2010)). The third category of models consists of a trade-off between the first two categories in terms of accuracy and computational efficiency. This kind of model uses two-state approximation of the thermal dynamics inside the cell and predicts the surface and the core temperatures of the cell Forgez et al (2010) and Park et al (2003). Here, we resort to the third category model for designing the diagnosis scheme.

In existing literature, Lithium-ion battery estimation problems have received a lot of attention in the past few years. Different state of charge (SOC) and state of health (SOH) estimation techniques have been proposed using equivalent circuit models (see Kim (2006) and Hu et al (2012)), and electrochemical models (see Dey et al (2015a) , Dey et al (2015b), Dey et al (2014a), Dey et al (2014b), Klein et al (2013) and Moura et al (2012)). Similarly, an adaptive estimation algorithm for a two-state thermal model has been presented in Lin et al (2013).

The fault diagnosis problems in Lithium-ion batteries are relatively less discussed in existing literature. Some existing approaches discuss sensor and actuator fault detection (see Marcicki et al (2010 and Liu et al (2014)) and Lombardi et al (2014)), over charge and over-discharge fault detection (see Singh et al (2013)). The authors of the present paper proposed sensor fault diagnosis scheme and electrochemical diagnostics scheme (see Dey et al (2015c) and Dey et al (2015d)). However, very few of existing approaches address internal thermal faults in the battery system. For example Marcicki et al (2010) and Liu et al (2014) used a one-state averaged thermal model for fault detection. However, as mentioned before, this one-state thermal model may not be able to capture the different internal thermal faults. In this paper, we extend this research by proposing a two-state thermal model-based diagnostics scheme that is able to detect

2405-8963
Peer review under responsibility of International Federation of Automatic Control.
10.1016/j.ifacol.2015.10.056

and isolate different internal thermal faults along with estimating the fault effects.

In this paper, we consider three different internal thermal faults, namely, thermal runaway, convective cooling resistance fault, and internal thermal resistance fault. A Luenberger observer is used for generating two primary residual signals that are used to detect and isolate different thermal faults. Further, based on the observer error dynamics, two secondary filters are designed, the input of which are the primary residuals. The outputs from the filters are treated as secondary residuals and essentially serve as estimates of the fault effects.

The rest of the paper is organized as follows: In section 2, the two-state thermal model of the battery is described, section 3 describes the proposed thermal fault diagnosis scheme. The simulation results are presented in section 4 and conclusion is derived in section 5.

2. THERMAL MODELING OF LITHIUM-ION BATTERY

2.1 Lithium-ion Battery Nominal Model

In this paper, the battery thermal model is radial in nature with a heat source in the core (see Forgez et al (2010), Park et al (2003) and Lin et al (2013)). The model consists of two states, the core temperature T_c and the surface temperature T_s such that

$$C_c\dot{T}_c = \frac{T_s - T_c}{R_c} + I^2R \tag{1}$$

$$C_s\dot{T}_s = -\frac{T_s - T_c}{R_c} + \frac{T_f - T_s}{R_u} \tag{2}$$

where R is the battery internal resistance, R_c is the thermal resistance between the core and surface, R_u is the convective cooling resistance between the surface and surrounding air and is a function of air coolant flow rate V, C_c is the heat capacity inside battery, C_s is the heat capacity of the battery surface material, and T_f is the air temperature of surrounding environment.

For battery electrical dynamics, we have considered a zeroth order equivalent circuit model that consists of an open-circuit voltage source and the internal resistance in series. The electrical dynamics can be obtained from Kirchhoff's law:

$$V = E_0 - IR \tag{3}$$

where V is the battery terminal voltage, and E_0 is the open-circuit voltage. Similarly, the State of Charge (SOC) dynamics of the battery can be written as:

$$\dot{SOC} = -I/Q \tag{4}$$

where Q is the battery capacity. Note that E_0 is a function of SOC and T_c. In this paper, we concentrate on the Hybrid Electric Vehicle application of the battery and consider a narrow SOC operating range. We assume the following expression of the E_0:

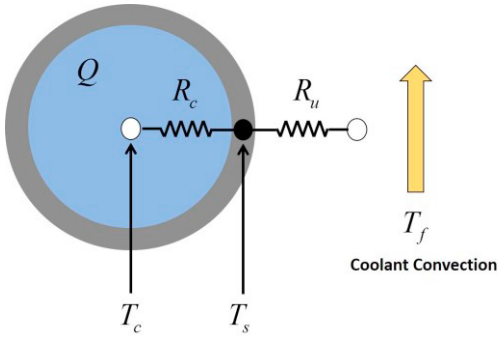

Figure 1: Battery lumped thermal modelling approach

$$E_0 = \alpha_0 + \alpha_1 SOC + \alpha_2 T_c \tag{5}$$

where α_0, α_1 and α_2 are constant parameters that can be determined apriori by offline identification techniques. We also assume that the internal resistance (R) of the battery is approximately constant and known with sufficient accuracy in the considered operating range.

2.2 Fault Modelling

In this paper, we consider three different thermal faults in the battery:

Fault 1: Convective cooling resistance fault, which is represented by a significant deviation in the parameter R_u from its nominal value.

Fault 2: Internal thermal resistance fault, which is modelled by change in the parameter R_c from its nominal value.

Fault 3: Thermal runaway fault, which is modelled by an additional heat-generation term that contributes to the core temperature rise in the battery. This is represented as an additional unknown input in the core temperature dynamics (1).

Considering these three faults, the faulty model of the battery can be written as:

$$C_c\dot{T}_c = \frac{T_s - T_c}{R_c + \Delta R_c} + I^2R + \Delta u \tag{6}$$

$$C_s\dot{T}_s = -\frac{T_s - T_c}{R_c + \Delta R_c} + \frac{T_f - T_s}{R_u + \Delta R_u} \tag{7}$$

where ΔR_u, ΔR_c and Δu represent *Fault 1, 2* and *3* respectively.

3. THERMAL DIAGNOSTIC SCHEME

First, we setup the diagnostics problem. The goal of the diagnostic scheme is to detect, isolate and if possible, provide some estimate of the thermal faults discussed in the previous section. The following assumptions are considered in designing steps:

Assumption 1: The on-board measurements from battery are surface temperature T_s, input current I and terminal voltage V. These measurements are NOT faulty.

Assumption *2*: Nominal values of all the battery parameters are known with sufficient accuracy.

Assumption 3: No multiple faults can occur at the same time. This assumption is required to facilitate the isolation of the faults.

Considering the faulty battery model (6), (7), and terminal voltage equation (3), the state-space model of the battery can be written as:

$$\dot{x} = Ax + B_1 u^2 + B_2 T_f + f \tag{8}$$

$$\begin{aligned} y_1 &= \alpha_0 + \alpha_1 SOC + \alpha_2 x_1 - uR \\ y_2 &= x_2 \end{aligned} \tag{9}$$

where $x = [x_1, x_2]^T$, $x_1 = T_c$, $x_2 = T_s$, $y_1 = V$, $u = I$ and $f = [f_1, f_2]^T$, $A = \begin{bmatrix} A_{11} & A_{12} \\ A_{21} & A_{22} \end{bmatrix}$, $A_{11} = -1/R_c C_c$, $A_{12} = 1/R_c C_c$, $A_{21} = -1/R_c C_s$, $A_{22} = -1/R_u C_s - 1/R_c C_s$, $B_1 = [1/C_c, 0]^T$, $B_2 = [0, 1/R_u C_s]^T$. Note that, f_1 and f_2 represent the lumped additive effect of the afore-mentioned faults. The mapping from the actual faults to f_1 and f_2 is given below:

Table 1: Fault mapping

Actual Faults	Fault Map
ΔR_u	$f_1 = 0, f_2 \neq 0$
ΔR_c	$f_1 \neq 0, f_2 \neq 0$
Δu	$f_1 \neq 0, f_2 = 0$

This mapping and the additive description of the faults in (8) and (9) will be useful for designing the diagnostic scheme. Essentially, we treat the problem in detecting, isolating and estimating f_1 and f_2 which is equivalent to detecting and isolating ΔR_u, ΔR_c and Δu faults. However, we will only be able to estimate f_1 and f_2, which are the lumped effects of the actual faults, not the exact actual faults (ΔR_u, ΔR_c and Δu).

The fault diagnosis scheme is shown in Fig. 2. The scheme is based on a Luenberger-type observer based on the battery nominal model (which is (8) and (9) with $f_1, f_2 = 0$). The observer generates two primary residuals (r_1 and r_2) that are used to detect and isolate f_1 and f_2. Then, these two primary residuals are passed through two filters and generate two secondary residuals (s_1 and s_2) which serve as estimates off_1 and f_2 respectively. The fault signature table is shown below.

Table 2: Fault signature table

r_1	r_2	Fault
1	0	f_1 (estimate is given by s_1)
0	1	f_2 (estimate is given by s_2)

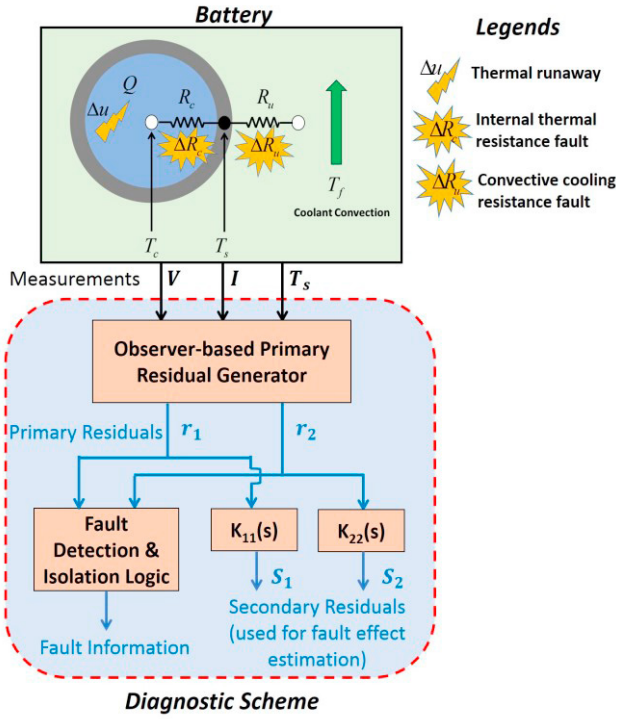

Figure 2: The diagnostic scheme

2.1 Primary Residual Generation

A Luenberger-type observer is used to generate the primary residuals. The observer structure is given by:

$$\dot{\hat{x}} = A\hat{x} + B_1 u^2 + B_2 T_f + L[\tilde{y}_1, \tilde{y}_2]^T \tag{10}$$

$$\begin{aligned} \hat{y}_1 &= \alpha_0 + \alpha_1 SOC + \alpha_2 \hat{x}_1 - uR \\ \hat{y}_2 &= \hat{x}_2 \end{aligned} \tag{11}$$

where $L = \begin{bmatrix} L_{11} & L_{12} \\ L_{21} & L_{22} \end{bmatrix}$ $\tilde{y}_1 = y_1 - \hat{y}_1$ and $\tilde{y}_2 = y_2 - \hat{y}_2$. We assume that correct SOC information is available via Coulomb-counting. Subtracting (10) and (11) from (8) and (9), the nominal error dynamics of the observer can be written as:

$$\dot{\tilde{x}} = A\tilde{x} - L[\tilde{y}_1, \tilde{y}_2]^T \tag{12}$$

where $\tilde{x} = [\tilde{x}_1, \tilde{x}_2]^T$ $\tilde{x}_1 = x_1 - \hat{x}_1$ and $\tilde{x}_2 = x_2 - \hat{x}_2$. Now, we choose $L_{12} = A_{12}$, $L_{21} = A_{21}/\alpha_2$ and choose L_{11} and L_{22} in such a way that $(A_{11} - L_{11}\alpha_2)$ and $(A_{22} - L_{22})$ will be negative and provide the desired convergence rate for estimation error. Note that, these choices of observer gains essentially leads to the following error dynamics of the individual states:

$$\begin{aligned} \dot{\tilde{x}}_1 &= (A_{11} - L_{11}\alpha_2)\tilde{x}_1 \\ \dot{\tilde{x}}_2 &= (A_{22} - L_{22})\tilde{x}_2 \end{aligned} \tag{13}$$

Note that, in presence of faults, the error dynamics can be written as:

$$\dot{\tilde{x}}_1 = (A_{11} - L_{11}\alpha_2)\tilde{x}_1 + f_1$$
$$\dot{\tilde{x}}_2 = (A_{22} - L_{22})\tilde{x}_2 + f_2 \quad (14)$$

Now, we define the two primary residuals as $r_1 = \tilde{y}_1$ and $r_2 = \tilde{y}_2$ and their dynamics can be written as:

$$\dot{\tilde{y}}_1 = \alpha_2\dot{\tilde{x}}_1 = (A_{11} - L_{11}\alpha_2)\tilde{y}_1 + \alpha_2 f_1$$
$$\dot{\tilde{y}}_2 = \dot{\tilde{x}}_2 = (A_{22} - L_{22})\tilde{x}_2 + f_2 \quad (15)$$

We can see from (15) that in presence of faults f_1 and f_2, the residuals r_1 and r_2 will be nonzero respectively. This satisfies the fault signature in Table 2.

2.1 Secondary Residual Generation

Based on (15), we generate the secondary residuals which serve as estimates of the faults f_1 and f_2. From (15), the transfer function from the faults to primary residuals can be written as:

$$G_{11}(s) = \frac{R_1(s)}{F_1(s)} = \frac{\alpha_2}{s - (A_{11} - L_{11}\alpha_2)}$$
$$G_{22}(s) = \frac{R_2(s)}{F_2(s)} = \frac{1}{s - (A_{22} - L_{22})} \quad (16)$$

where $R_1(s)$, $R_2(s)$, $F_1(s)$ and $F_2(s)$ are Laplace transforms of r_1, r_2, f_1 and f_2, respectively. Based on (16), we can write that:

$$K_{11}(s) = \frac{S_1(s)}{R_1(s)} = \frac{s - (A_{11} - L_{11}\alpha_2)}{\alpha_2(\tau_1 s + 1)}$$
$$K_{22}(s) = \frac{S_2(s)}{R_2(s)} = \frac{s - (A_{22} - L_{22})}{(\tau_2 s + 1)} \quad (17)$$

where s_1 and s_2 are the secondary residuals. We can see from (17) that K_{11} and K_{22} are two filters, the inputs of which are primary residuals r_1 and r_2 and the outputs are essentially estimates of f_1 and f_2. The parameters τ_1 and τ_2 are design parameters chosen to make the filter structure proper.

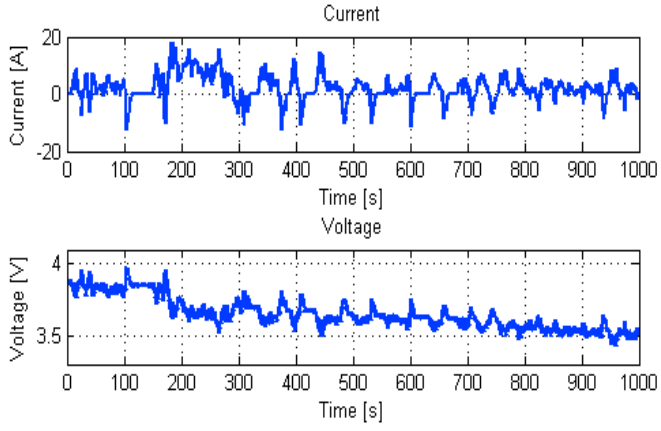

Figure 3: Current and Voltage response of scaled version of UDDS drive-cycle

4. SIMULATION STUDIES

In this section, we present a simulation study to verify the effectiveness of the proposed scheme. The battery model parameters are taken from [17]. First, a nominal case has been shown with a current profile derived from scaled version of UDDS drive cycle (Fig. 3). The core and surface temperature estimation performance and primary residuals are shown in Fig. 4. Note that the primary residuals converge to zero as there are no faults.

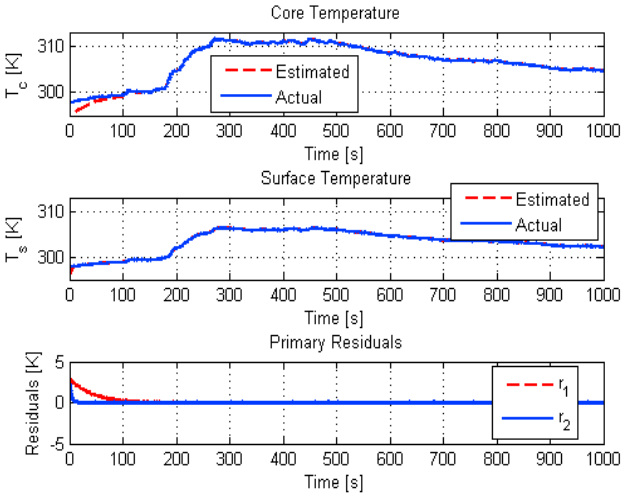

Figure 4: Core and surface temperature estimation performance in nominal case (no faults).

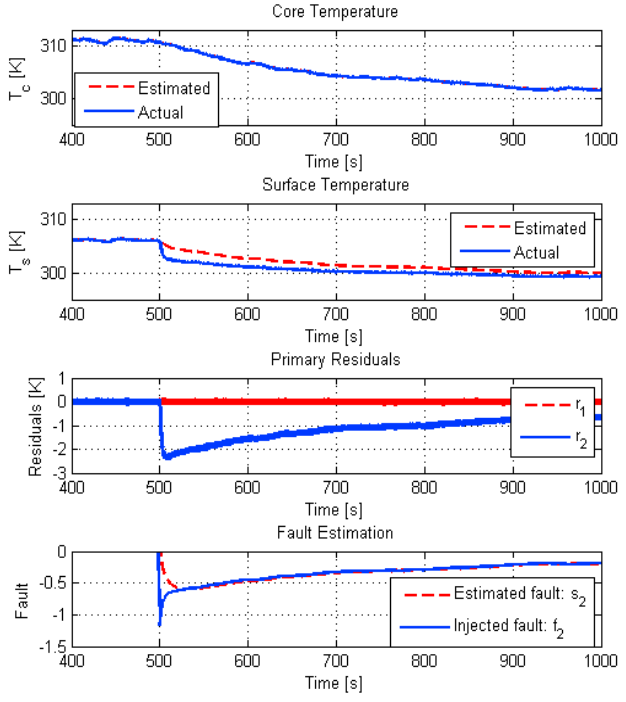

Figure 5: Residual responses in case of ΔR_u fault.

Next, we consider ΔR_u fault case. A step change as $\Delta R_u = 0.3R_u$ is injected at t=500 sec. The core and surface temperature estimation performance along with the residual is shown in Fig. 5. As expected, r_2 goes nonzero and r_1 remains zero as this fault generates a condition $f_1 = 0, f_2 \neq 0$. Further, the effect of the fault is estimated by secondary residual s_2.

In the next study, we consider Δu fault case. A step change as Δu is injected at t=500 sec. The core and surface temperature estimation performance along with the residual is shown in Fig. 6. As expected, r_1 goes nonzero and r_2 remains zero as this fault generates a condition $f_1 \neq 0, f_2 = 0$. Further, the effect of the fault is estimated by secondary residual s_1.

In the final case, we consider ΔR_c as the fault. A step change as $\Delta R_c = 0.2R_c$ is injected at t=500 sec. The core and surface temperature estimation performance along with the residual is shown in Fig. 7. As expected, both r_1 and r_2 goes nonzero as this fault generates a condition $f_1 \neq 0, f_2 \neq 0$. Further, the effect of the fault is estimated by secondary residuals s_1 and s_2.

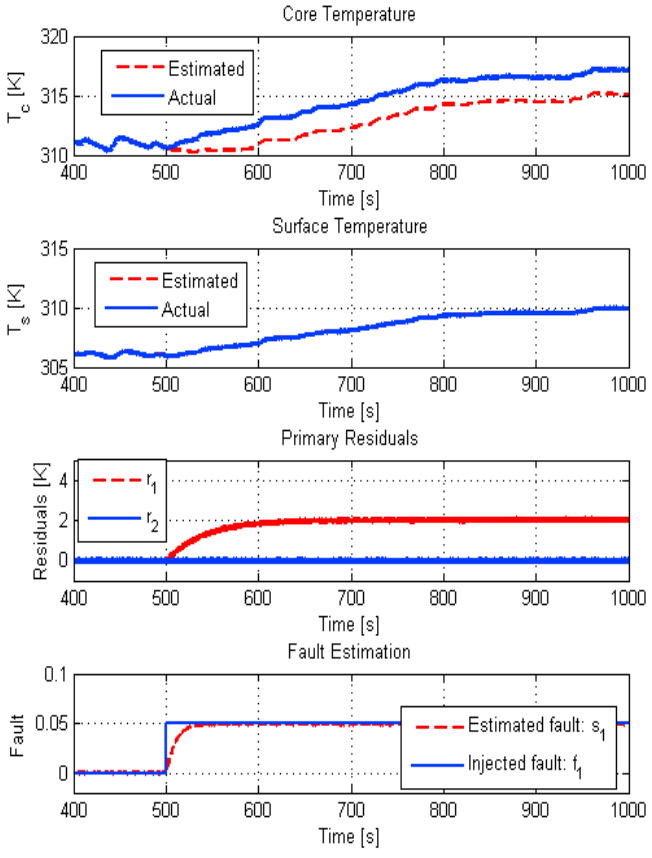

Figure 6: Residual responses in case of Δu fault.

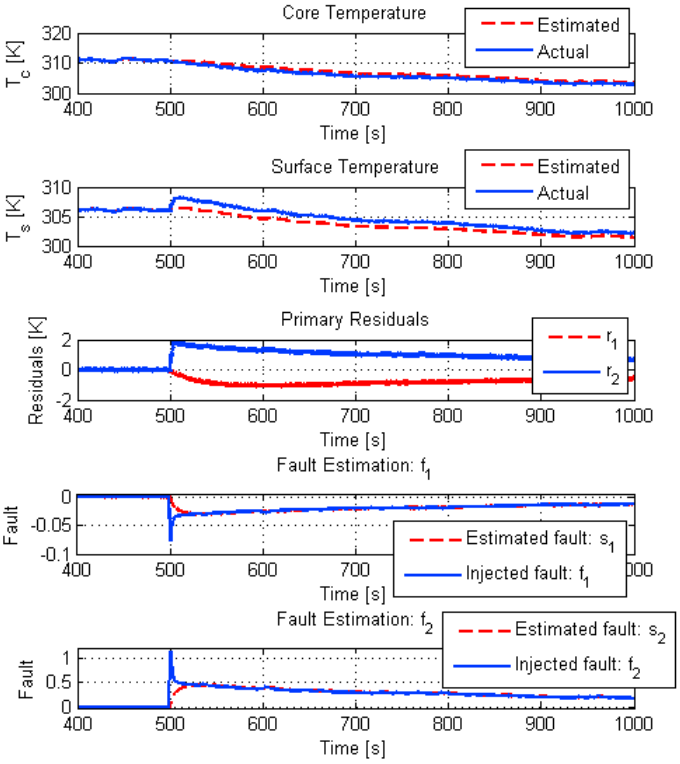

Figure 7: Residual responses in case of ΔR_c fault.

5. CONCLUSION

In this paper, Lithium-ion battery is modelled via equivalent circuit model and a two-state thermal model is considered to capture thermal dynamics of the battery. A diagnosis scheme based on Luenberger observer has been proposed to detect and isolate thermal runaway, convective cooling resistance fault, and internal thermal resistance fault, as three possible internal thermal failures. In addition, the secondary residuals are derived using designed filters and primary residuals to estimate the additive effect of the possible faults in the battery.

ACKNOWLEDGEMENTS

Research supported by the US Department of Energy GATE program under grant number DE-EE0005571.

REFERENCES

Dey, S., Ayalew, B. and Pisu, P. (2015). Nonlinear Robust Observers for State-of-Charge Estimation of Lithium-Ion Cells Based on a Reduced Electrochemical Model. *IEEE Transactions on Control Systems Technology*, available online, DOI: 10.1109/TCST.2014.2382635.

Dey, S., Ayalew, B. and Pisu, P. (2015). Nonlinear Adaptive Observer for a Lithium-ion Battery Cell Based on Coupled Electrochemical-Thermal Model. *ASME Journal of Dynamic Systems, Measurement, and Control*, available online, DOI: 10.1115/1.4030972.

Dey, S., Ayalew, B. and Pisu, P. (2014). Adaptive Observer Design for a Li-Ion Cell Based on Coupled Electrochemical-Thermal Model. In the *Proceedings of 2014 ASME Dynamic Systems and Control Conference (DSCC),* pp. V002T23A001.

Dey, S., Ayalew, B., and Pisu, P. (2014). Combined Estimation of State-of-Charge and State-of-Health of Li-ion Battery Cells Using SMO on Electrochemical Model. In *13th International Workshop on Variable Structure Systems*, pp. 1-6.

Dey, S., Mohon, S., Pisu, P and Ayalew, B. (2015). Sensor Fault Detection, Isolation and Estimation in Li-ion Batteries. Submitted to *IEEE Transactions on Control Systems Technology*.

Dey, S., and Ayalew, B. (2015). Observer-based Diagnostic Scheme for Detection, Isolation and Estimation of Electrochemical Faults in Lithium-ion Cells. submitted to *ASME 2015 Dynamic Systems and Control Conference*.

Divya. K.C. and Ostergaard. J. (2009). Battery energy storage technology for power systems—an overview. *Journal of Electric Power Systems Research*, pp. 511–520.

Forgez, C. , Do, D. V., Friedrich, G., Morcrette, M. and Delacourt, C. (2010). Thermal modeling of a cylindrical lifepo4/graphite lithium-ion battery, *Journal of Power Sources*. vol. 195, pp. 2961–2968.

Gu, W. B., and Wang, C. Y. (2000). Thermal-electrochemical modeling of battery systems. *Journal of The Electrochemical Society*, vol. 147, pp. 2910–2922.

Hallaj, S. A., Maleki, H., Hong, J., and Selman, J. (1999). Thermal modeling and design considerations of lithium-ion batteries. *Journal of Power Sources*, vol. 83, pp. 1–8.

Hu, Y., and Yurkovich, S. (2012). Battery cell state-of-charge estimation using linear parameter varying system techniques. *Journal of Power Sources*, vol. 198, pp. 338–350.

Kim, I.-S. (2006).The novel state of charge estimation method for lithium battery using sliding mode observer. *Journal of Power Sources*, vol. 163, no. 1, pp. 584–590.

Klein, R., Chaturvedi, N. A., Christensen, J., Ahmed, J., Findeisen, R., and Kojic, A. (2013). Electrochemical Model Based Observer Design for a Lithium-Ion Battery. *IEEE Transactions on Control Systems Technology*, vol. 21, no. 2, pp. 289-301.

Lin, X. , Perez, H. E. , Siegel, J. B. , Stefanopoulou, A. G. , Li, Y., Anderson, R.D. , Ding, ,Y., and Castanier, M. P. (2013). Online parameterization of lumped thermal dynamics in cylindrical Lithium ion batteries for core temperature estimation and health monitoring. *IEEE transaction on control system technology*, vol. 21, no. 5, pp. 1745-1755, September.

Liu, Z., Ahmed, Q., Rizzoni, G., and He, H. (2014). Fault Detection and Isolation for Lithium-Ion Battery System Using Structural Analysis and Sequential Residual Generation. In the *Proceedings of 2014 ASME Dynamic Systems and Control Conference (DSCC),* pp. V002T36A005.

Lombardi, W., Zarudniev, M., Lesecq, S., and Bacquet, S. (2014). Sensors fault diagnosis for a BMS. In *2014 European Control Conference (ECC)*, pp. 952-957.

Maleki, H., and Shamsuri, A. K. (2003). Thermal analysis and modeling of a notebook computer battery. *Journal of Power Sources*, vol. 115, pp. 131–136.

Marcicki, J., Onori, S., and Rizzoni, G. (2010). Nonlinear fault detection and isolation for a lithium-ion battery management system. In *ASME 2010 Dynamic Systems and Control Conference*, pp. 607-614.

Moura, S. J., Chaturvedi, N. A., and Krstic, M. (2012). PDE estimation techniques for advanced battery management systems—Part I: SOC estimation. In *2012 American Control Conference (ACC)*, pp. 559-565.

Park C. W. and Jaura, A. K. (2003). Dynamic thermal model of li-ion battery for predictive behavior in hybrid and fuel cell vehicles. *SAE 2003-01-2286*.

Singh, A., Izadian, A., and Anwar, S. (2013). Fault diagnosis of Li-Ion batteries using multiple-model adaptive estimation. In *IECON 2013-39th Annual Conference of the IEEE*, pp. 3524-3529.

Smith, K., and Wang, C.-Y. (2006). Power and thermal characterization of a lithium-ion battery pack for hybrid-electric vehicles. *Journal of Power Sources*, vol. 160, p. 662-673.